An X-ray Absorption Spectroscopy Investigation of the Formation of FeCo Alloy Nanoparticles in Al_2O_3 Xerogel and Aerogel Matrixes

Anna Corrias,*,† Gabriele Navarra,† Maria F. Casula,† Sergio Marras,† and Gavin Mountjoy‡

Dipartimento di Scienze Chimiche, Università di Cagliari, Cittadella Universitaria di Monserrato, Strada Statale 554 bivio per Sestu, 09042 Monserrato, Cagliari, Italy, and School of Physical Sciences, University of Kent, Canterbury, CT2 7NR, U.K.

Received: March 8, 2005; In Final Form: June 1, 2005

Extended X-ray absorption fine structure and X-ray absorption near-edge structure techniques were used to study in detail the structural characteristics of FeCo−Al_2O_3 nanocomposite xerogels and aerogels. The formation of bcc FeCo alloy, which cannot be assessed unambiguously by X-ray diffraction, dispersed within the alumina matrix was evidenced in the final samples obtained by heat treatment at 800 °C in reducing atmosphere. Aerogel samples reduced below 800 °C still present a fraction of oxidized metal together with the bcc alloy. The investigation of the xerogels and aerogels calcined at increasing temperature indicates that Fe(III) and Co(II) ions are present and they are located in the tetrahedral sites of the spinel structure of the matrix (γ-Al_2O_3); moreover, the precursor of the spinel is more ordered in the aerogel sample than the xerogel sample.

Introduction

Nanocomposites composed of transition metal nanoparticles embedded in an inorganic matrix are regarded as promising for the design of catalytically and magnetically active materials.[1] Recently attention has turned to supported bimetallic nanoparticles with the aim of increasing the stability of the metallic phase or to obtain new or enhanced properties.[2]

Supported FeCo alloy nanoparticles dispersed into insulating matrixes are of interest in view of their improved catalytic performance[3,4] and of their size-dependent soft magnetic properties.[5,6] These materials can be prepared using the sol−gel process by co-gelling the suitable hydrolyzable precursors for the matrix and for the FeCo nanoparticles.[7] Mixing at the molecular level in the initial sol and controlled co-gelation of the precursors allow one to achieve a good homogeneity in terms of both composition and distribution of the dispersed phase within the matrix. Moreover, the appropriate gel deposition and drying technique allows one to prepare nanocomposites in different forms; for instance, FeCo−SiO_2 xerogels, aerogels, and films have been prepared.[8−11]

More recently the sol−gel method has been successfully applied to the preparation of FeCo−Al_2O_3 nanocomposites, in which the different matrix is expected to play a significant role not only in the formation and growth of the dispersed nanoparticles but also on the magnetic properties of the resulting material.[12]

The nanocomposite formation starting from the gel occurs via a number of stages, which include the calcination of the gel, to get rid of the synthesis byproducts and unreacted reagents and to promote nanoparticle formation, and the reduction treatment, to obtain metallic nanoparticles. Understanding of the structural evolution of the gel at the different stages is a key factor for the successful preparation of the resulting nanocomposite by adopting the appropriate post-gelation treatments. The structural characterization of the samples performed by X-ray diffraction suggested that under oxidizing conditions a phase with a spinel structure similar to γ-Al_2O_3 is obtained. Under reducing conditions FeCo−Al_2O_3 nanocomposites constituted by FeCo alloy nanoparticles dispersed in nanocrystalline γ-Al_2O_3 are obtained. [12]

However, due to the low concentration of the nanocrystalline metal phase with respect to the matrix and to the difficulty of discriminating cobalt and iron, which have very similar X-ray scattering factors, a detailed study of the nature of the products formed at the different stages of the preparation requires the use of experimental techniques that can selectively study the environment of the two metals.

X-ray absorption techniques are very suitable structural tools because they are elemental specific, hence can examine the Fe and Co atom environments separately, and can give valuable information in the case of dilute and disordered samples.[13] Quantitative structural information about the metal atom environment in complex materials can be obtained from extended X-ray absorption fine structure (EXAFS) spectra in terms of number and type of neighboring atoms around a selected absorbing atom, interatomic distances, and Debye−Waller factors. X-ray absorption near-edge structure (XANES) can also provide information about the metal atom environment. The use of these techniques has already provided valuable information for the study of metal oxide nanoparticles and nanocomposites prepared by the sol−gel process.[14−19]

In this paper the use of X-ray absorption spectroscopy for the structural characterization of the Fe and Co environment in FeCo−Al_2O_3 xerogels and aerogels at different stages of the sol−gel process is presented.

Experimental Section

Sample Preparation. FeCo−Al_2O_3 gels were prepared using aluminum tri-*sec*-butoxide ($Al(OC_4H_9^{sec})_3$, Aldrich 97%, ASB) and metal nitrates ($Fe(NO_3)_3 \cdot 9H_2O$, Aldrich, 98%, $Co(NO_3)_2 \cdot 6H_2O$, Aldrich, 98%) as precursors and ethanol (Carlo Erba

* To whom correspondence should be addressed. Tel: +39 070 6754351. Fax: +39 070 6754388. E-mail: corrias@unica.it.
† Università di Cagliari.
‡ University of Kent.

10.1021/jp051193l CCC: $30.25
Published on Web 07/06/2005

99.8%, EtOH) as solvent.[12] The total metal amount in the final nanocomposite was 10 wt % (Fe+Co/Fe+Co+Al_2O_3), and the Fe/Co molar ratio was 1/1 for all samples.

To obtain the aerogel samples, the alcogels were submitted to high-temperature supercritical drying in an autoclave (Parr, 300 cm^3) filled with an appropriate amount of ethanol. After supercritical drying, the aerogels were calcined at 450 °C in static air for 1 h and then either further calcined at 900 °C or reduced under H_2 flow at temperatures between 700 and 800 °C from 2 to 12 h. Xerogels were obtained by submitting the alcogel to a calcination treatment in static air for 1 h at 450 °C; after this treatment the sample was either further calcined at 900 °C for 1 h or reduced under H_2 flow at 800 °C for 2 h.

Data Collection. The X-ray absorption spectroscopy experiments were carried out on station 9.2 of the SRS, Daresbury Laboratory, U.K. Data at the Fe and Co K-edges were collected in transmission mode at room temperature on xerogel and aerogel samples treated in air and in hydrogen flow and on some reference compounds. Samples with a suitable and highly uniform optical thickness were prepared from powders; in the case of the xerogel and reference samples the powders were dispersed in an inert solvent and then filtered onto polythene supports. In the case of the aerogel samples the powders were pressed into pellets without the need of using any diluent, the aerogels being very easy to compress due to their very low apparent density.

Ion chambers before and after the samples were used to measure the incident and transmitted intensities, I_0 and I_t, respectively. A double Si(111) monochromator was used; higher order harmonic rejection was achieved by detuning the monochromator so that the transmitted flux was reduced by 50%. In the EXAFS region, absorption was measured at constant k intervals. In the XANES region, absorption was measured at intervals of approximately 0.25 eV. The resolution of the monochromator is approximately 1 eV in the energy range studied. The energy scale was calibrated to an accuracy of 0.5 eV by simultaneously measuring the absorption through 5 μm thick Fe or Co foils, by using a third ion chamber. The energy of the first inflection point for Fe and Co foils was taken to be 7112 and 7709 eV, respectively.[20]

EXAFS Data Analysis. The program Viper was used to identify the beginning of the absorption edge, E_0, to fit pre-edge and post-edge backgrounds, μt_{pre} and μt_{post}, respectively, and hence to obtain the normalized absorbance $\chi = (\mu t - \mu t_{post})/(\mu t_{post} - \mu t_{pre})$.[21]

Structural information was obtained using EXCURV98 to model the experimental $\chi(k)$ using fast curved wave theory [22] where

$$\chi(k) = \sum_i S_0^2(k)(N_i/kR_i^2)|f_i(k,R)| \sin(2kR_i + 2\delta(k) + \varphi_i(k,R)) \exp(-2\sigma_i^2 k^2) \exp(-2R_i/\lambda(k)) \quad (1)$$

and k is the modulus of the wave-vector of the photoelectron, and R_i, N_i, and $2\sigma_i^2$ are the distance, coordination number, and Debye−Waller term (due to static and thermal disorder) for the ith shell of neighboring atoms. The additional parameters in eq 1 are the effective curved wave backscattering amplitude $f(k,R)$ of the scatterer, the phase shift due to the absorbing atom potential $2\delta(k)$, the phase shift due to the scatterer $\varphi_i(k,R)$, and the inelastic mean free path of the photoelectron $\lambda(k)$.

The fitting was carried out in k-space in the range 2.5 to about 12 $Å^{-1}$, which is the upper accessible k value at the Fe K-edge because of the presence of the Co K-edge; the same k range was used at the Co edge to achieve a similar resolution. Theoretical parameters $|f_i(k,R_i)|$, $\varphi_i(k,R_i)$, $\delta(k)$, and $\lambda(k)$ were calculated using the von Barth potential for ground states, the Hedin−Lundquist exchange potential for excited states,[23] and the relaxed approximation for the core-hole.[24] In EXCURV98 the k-independent parameter AFAC takes the place of $S_0(k)^2$ in eq 1. AFAC was determined to be 0.9 from fitting to the reference samples. The parameter EF, which is a correction to E_0, was free to vary in all fitting.

Equation 1 is valid for single scattering of the photoelectron. However, multiple scattering can be significant depending on the structure.[25] fcc and bcc lattices are examples of compounds where multiple scattering is expected to be particularly strong for certain shells due to a forward-scattering path (also called the focusing or shadowing effect) consisting of collinear arrangements of neighboring atoms.[26] When necessary, the effect of multiple scattering was included by calculating all the multiple scattering paths within clusters centred on the central atom, using the Rehr and Albers approximation.[27,28]

The structural parameters were obtained by nonlinear least-squares fitting in k-space with a k^3 weighting of the total experimental EXAFS spectra. The quality of the fit was judged from the normalized sum of residuals

$$R\text{-factor} = \sum_n |k_n^3 \chi_{expt}(k_n) - k_n^3 \chi_{fit}(k_n)| / \sum_n |k_n^3 \chi_{expt}(k_n)| \times 100 \quad (2)$$

While reasonable EXAFS fits of single shells typically have values below 20%, when the fit is performed on the total EXAFS spectra, higher values can still correspond to good fits, especially if the fit is not extended to peaks at high R. The errors in the fit parameters, R_i, N_i, and $2\sigma_i^2$, were obtained from the 95% confidence level as calculated in EXCURV98.[29]

XANES Data Analysis. The XANES spectra were processed in the usual way to obtain normalized absorbance.[30] XANES at the K-edge involves the excitation of a 1s photoelectron into low-lying empty states at the central atom with p-type symmetry. The characteristic features of the XANES spectra for transition metal oxides[20] are as follows. An increase in valence of the metal atom causes a shift to higher energies. Pre-edge peak(s) may occur corresponding to 1s to 3d transitions with 3d−4p mixing. The pre-edge peak increases in intensity as the degree of centrosymmetry of the metal atom environment decreases. The main peak and shoulders of the absorption edge correspond to transitions to 4p continuum states and "shape resonances" of the metal atom environment. For a given environment, the main peak is broadened by disorder in the nearest neighbor distances. Secondary peaks occurring a few 10 eV above the main peak correspond to multiple scattering from neighboring atom shells.

Results and Discussion

Calcined Samples. Figure 1 shows the Fe and Co K-edge $k^3\chi(k)$, and the corresponding Fourier transforms (FT), for the aerogel and xerogel samples calcined at 450 and 900 °C. As a comparison, the data of the γ-Fe_2O_3 and $CoAl_2O_4$ reference compounds are also shown.

The $k^3\chi(k)$ at the Fe K-edge for the xerogel and aerogel samples calcined at both 450 and 900 °C present broad oscillations that are typical of disordered and low symmetry structures. Small differences can be noticed between the xerogel and the aerogel calcined at 450 °C. In particular, the main FT peak of the xerogel sample seems more symmetric than that of the aerogel. The calcination at 900 °C gives rise to slightly more structured functions in both the xerogel and aerogel samples,

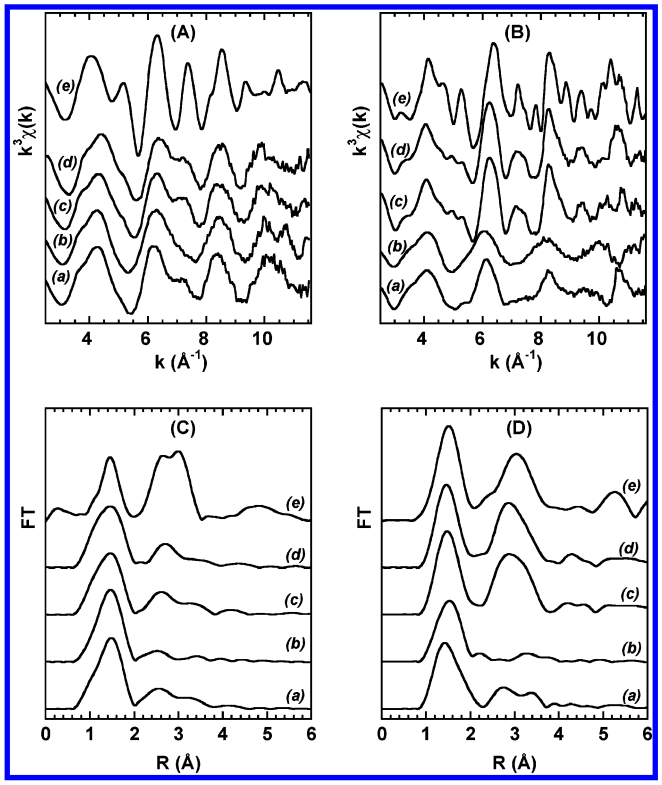

Figure 1. Experimental $k^3\chi(k)$ at the (A) Fe and (B) Co K-edge and corresponding FTs (not corrected for phase shift) at the (C) Fe and (D) Co K-edge for the calcined samples: (a) aerogel at 450 °C, (b) xerogel at 450 °C, (c) aerogel at 900 °C, (d) xerogel at 900 °C; (e) data of reference compounds, γ-Fe_2O_3 and $CoAl_2O_4$, are also shown for comparison.

as it can also be inferred from their FTs, which show some weak but evident peaks above the first peak. Even if the spectra of the calcined samples at the Fe K-edge do not show a close resemblance with any of the reference compounds, some features typical of spinel structures can be identified, as it can be inferred from the comparison with the spectrum of γ-Fe_2O_3. At the Co K-edge a more pronounced evolution with calcination temperature can be noticed; in both the xerogel and aerogel samples the treatment at 900 °C gives rise to a much more structured environment compared to the samples calcined at 450 °C, as also detectable from the corresponding FTs, where an intense peak is present at about 3 Å. The comparison with the spectrum of $CoAl_2O_4$ indicates a close similarity and therefore suggests that the cobalt environment in the samples calcined at 900 °C is similar to this compound. It should be pointed out that for $k > 10$ Å^{-1} the data for samples calcined at 450 °C, i.e., the less structured samples, have some sudden jumps as a likely consequence of monochromator glitches in addition to noise.

Figure 2 shows the Fe and Co K-edge XANES of oxide reference compounds. The XANES show differences in pre-edge peak (degree of centrosymmetry), main edge position (valence), and shape of main edge peak and shoulders (geometry of local environment). Figure 3 shows the Fe and Co K-edge XANES of aerogels and xerogels after calcination at 450 and 900 °C. The results indicate that in all samples only Fe(III) and Co(II) are present. After calcination at 900 °C the xerogel and aerogel have similar Co K-edge XANES and also similar Fe K-edge XANES. In comparison to reference compounds the Co K-edge XANES are most similar to $CoAl_2O_4$. (The shape of the pre-edge peak is not similar to $CoFe_2O_4$ or CoO, and the main edge position is not similar to Co_3O_4.) In comparison to reference compounds the Fe K-edge XANES are most similar

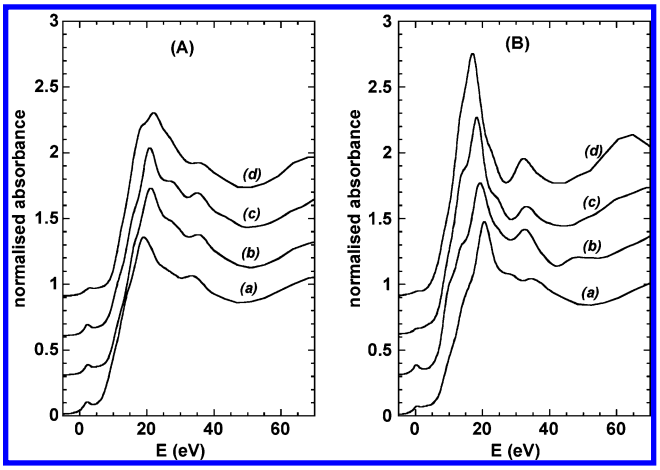

Figure 2. XANES spectra of oxide reference compounds. (A) Fe K-edge of (a) Fe_3O_4, (b) γ-Fe_2O_3, (c) $CoFe_2O_4$, (d) α-Fe_2O_3, and (B) Co K-edge of (a) Co_3O_4, (b) $CoAl_2O_4$, (c) $CoFe_2O_4$, (d) CoO.

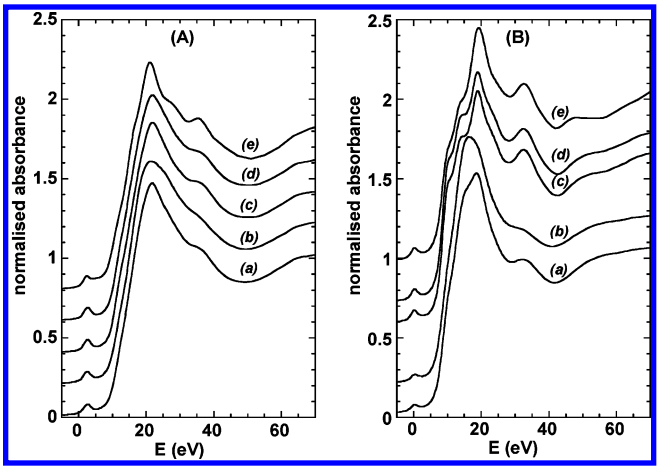

Figure 3. XANES spectra of calcined samples at the (A) Fe and (B) Co K-edge: (a) aerogel at 450 °C, (b) xerogel at 450 °C, (c) aerogel at 900 °C, (d) xerogel at 900 °C; (e) data of reference compounds, γ-Fe_2O_3 and $CoAl_2O_4$, are also shown for comparison.

to γ-Fe_2O_3 or $CoFe_2O_4$. (The shape of the pre-edge peak is not similar to α-Fe_2O_3, and the main edge position is not similar to Fe_3O_4.)

After calcination at 900 °C the xerogel and aerogel have quite similar Fe K-edge XANES and also quite similar Co K-edge XANES. The Fe K-edge XANES of aerogel calcined at 450 °C is similar to that at 900 °C, whereas the Co K-edge XANES of aerogel calcined at 450 °C has less sharp features than that at 900 °C and corresponds to a more disordered local environment. The Fe K-edge and Co K-edge XANES of the xerogel calcined at 450 °C both have less sharp features than those at 900 °C and correspond to more disordered local environments. Moreover, the Fe and Co K-edge XANES of xerogel calcined at 450 °C both have significantly less sharp features than in aerogel calcined at 450 °C, corresponding to more disordered local environments.

The qualitative comparison of the experimental EXAFS and XANES spectra at both the iron and cobalt edge with those of the reference compounds gives some valuable hints, which were used as a basis for fitting the total EXAFS spectra. The theoretical backscattering and phase shifts calculated by EXCURV98 were first checked on the reference compound data. The results of the fitting of different iron and cobalt oxides were presented in previous studies.[18,19] In addition, the fitting was performed on a $CoAl_2O_4$ reference compound which has a spinel

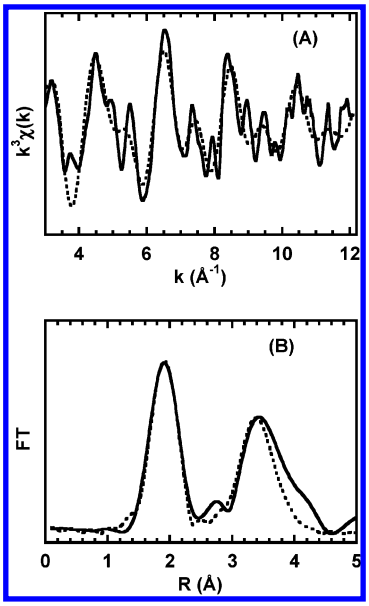

Figure 4. (A) $k^3\chi(k)$ spectra from experiment (—) and fit results (- - -) for the $CoAl_2O_4$ reference sample and (B) corresponding FT (corrected for phase shift).

TABLE 1: Interatomic Distances (R), Coordination Numbers (N), and Debye−Waller Factors (σ) from Fit of the $CoAl_2O_4$ Reference Compound[a]

atom	R (Å)	N	$2\sigma^2$ (Å^2)
O	1.95 (1)	4	0.009 (1)
Al	3.27 (3)	12	0.06 (1)
Co	3.49 (1)	4	0.013 (3)
R-factor	48%		

[a] Errors shown in parentheses for the parameters free to vary during fitting.

structure.[31] For a normal spinel all Co^{2+} would be in tetrahedral sites and all Al^{3+} in octahedral sites. However, some degree of inversion is reported for this structure, with up to 30% of the Co^{2+} in octahedral sites. Fitting was first carried out considering the sample to be a normal spinel, keeping N_i fixed, allowing small variations of the R_i values within the experimental error; the $2\sigma_i^2$ parameters were free to vary together with EF and AFAC.

The results of the fitting are shown in Figure 4, and the best fitting parameters are reported in Table 1. The fit is quite reasonable in the range of distances (up to 4 Å) introduced in the calculation, confirming that the calculated phase shifts and amplitudes can be used to fit the data of the samples at the Co edge. The results of the fitting carried out considering the $CoAl_2O_4$ structure to be partially inverted did not give rise to a significant improvement to justify the use of a larger number of free parameters. However, the presence of a small peak at about 2.9 Å in the FT is consistent with the presence of some Co^{2+} in octahedral sites. In fact, 2.86 Å is the distance between two octahedral sites. It should be noted that the Debye−Waller factors for the Co−Al distances are significantly larger than those for the Co−O and Co−Co ones.

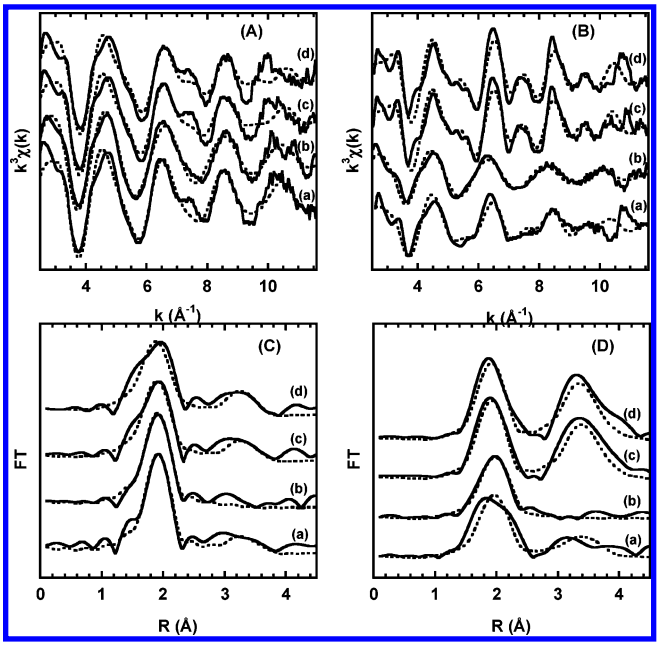

Figure 5. $k^3\chi(k)$ spectra from experiment (—) and fit results (- - -) at the (A) Fe and (B) Co K-edge and corresponding FTs (phase shift corrected) at the (C) Fe and (D) Co K-edge, for the (a) aerogel sample and (b) xerogel sample calcined at 450 °C and for the (c) aerogel sample and (c) xerogel sample calcined at 900 °C.

In Figure 5 the results of the fitting at the Fe and Co K-edges for the samples calcined at 450 and 900 °C are shown. In Table 2 the best fitting parameters are reported. Since coordination numbers and Debye−Waller factors are strongly correlated, coordination numbers were kept fixed in the final stages of the fitting procedure.

The results of the fitting indicate that in the xerogel sample calcined at 450 °C the Fe(III) and Co(II) occupy very disordered/low-symmetry sites since a reasonable fit is obtained with a single shell of oxygens. The aerogel calcined at the same temperature is much more structured and the environment is

TABLE 2: Interatomic Distances (R), Coordination Numbers (N), and Debye−Waller Factors (σ) from Fitting the EXAFS Spectra at the Fe and Co K-Edge for the Aerogel and Xerogel Samples Calcined at 450 and 900 °C[a]

	aerogel 450°C			xerogel 450°C			aerogel 900°C			xerogel 900°C		
					Fe K-edge							
atom	R (Å)	N	$2\sigma^2$ (Å^2)	R (Å)	N	$2\sigma^2$ (Å^2)	R (Å)	N	$2\sigma^2$ (Å^2)	R (Å)	N	$2\sigma^2$ (Å^2)
O	1.97 (1)	4	0.011 (2)	1.97 (1)	4	0.013 (2)	1.96 (1)	4	0.019 (2)	1.95 (1)	4	0.020 (2)
Al	3.34 (3)	3	0.023 (3)				3.32 (3)	3	0.019 (3)	3.31 (3)	3	0.016 (3)
R-factor		29%			26%			34%			38%	
					Co K-edge							
atom	R (Å)	N	$2\sigma^2$ (Å^2)	R (Å)	N	$2\sigma^2$ (Å^2)	R (Å)	N	$2\sigma^2$	R (Å)	N	$2\sigma^2$ (Å^2)
O	2.01 (1)	4	0.017 (1)	2.03 (1)	4	0.017 (1)	1.97 (1)	4	0.013 (1)	1.97 (1)	4	0.014 (1)
Al	3.33 (3)	5	0.05 (1)				3.35 (3)	12	0.05 (1)	3.35 (3)	12	0.04 (1)
Co	3.48 (1)	1.6	0.017 (3)				3.49 (1)	4	0.017 (3)	3.48 (1)	4	0.018 (3)
R-factor		51%			34%			45%			46%	

[a] Errors shown in parentheses for the parameters free to vary during fitting.

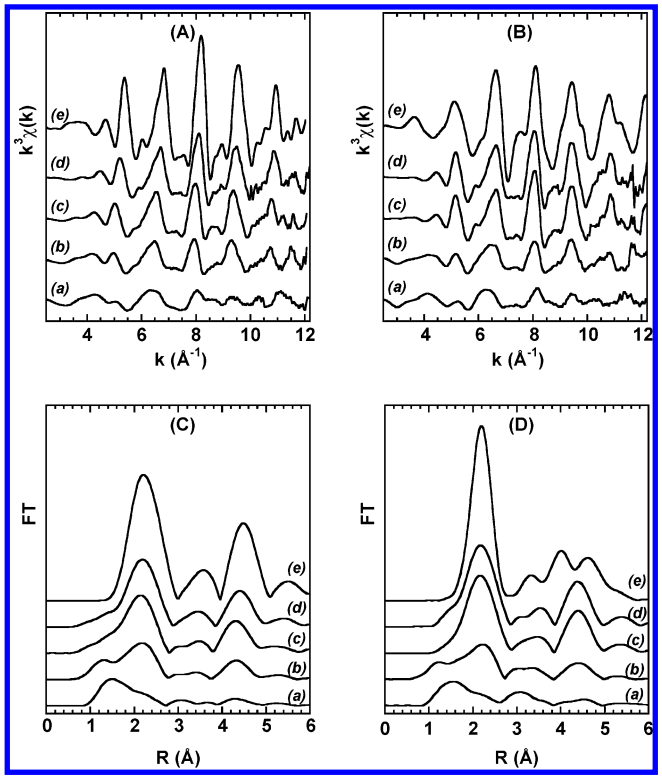

Figure 6. $k^3\chi(k)$ at the (A) Fe and (B) Co K-edge and corresponding FTs (not corrected for phase shift) at the (C) Fe and (D) Co K-edge, for the aerogels reduced at (a) 700 °C for 2 h, (b) 700 °C for 12 h, (c) 800 °C for 2 h, (d) for the xerogel reduced at 800 °C for 2 h, and (e) for the reference metal foils.

quite similar to the one observed in both xerogel and aerogel samples after calcinations at 900 °C. The results for the latter samples are consistent with both the Fe(III) and Co(II) being located in the tetrahedral sites of a spinel structure. However, the Fe(III) seems to be randomly distributed since the best fit was obtained considering only Fe−Al second shell distances, while Co(II) seems to be located into domains with a structure very similar to $CoAl_2O_4$, since both Co−Al and Co−Co interactions had to be introduced in the fit.

This results indicate quite a different evolution with calcination compared to FeCo−SiO_2 nanocomposites where calcination gave rise to the formation of iron and cobalt oxide nanoparticles which did not exhibit strong interactions with the matrix.[19]

Samples Reduced in H_2 Flow. In Figure 6 the Fe and Co K-edge $k^3\chi(k)$, and the corresponding FTs, for the aerogels reduced at 700 °C for 2 and 12 h, and at 800 °C for 2 h, and for the xerogel reduced at 800 °C for 2 h, are shown. As a comparison, the data of the bcc Fe and fcc Co foils are also shown.

The $k^3\chi(k)$ and FT of bcc Fe are significantly different from those of fcc Co, confirming that inspection of the EXAFS data of the reduced samples can give a straightforward indication on the formation of the bcc FeCo alloy. In fact, if the bcc FeCo alloy is formed, the data at both Fe and Co K-edges should be very similar to those of bcc Fe. This is indeed what is observed for both the xerogel and aerogel samples reduced at 800 °C for 2 h; their $k^3\chi(k)$ and corresponding FTs at the Fe and Co edge look very similar to each other and to bcc Fe. The samples reduced at 800 °C are therefore dominated by the presence of the bcc FeCo phase, and there are only minor differences between the data of the xerogel and aerogel samples. On the other hand, in FeCo−SiO_2 samples the formation of the FeCo alloy was found to be easier in the aerogel samples compared

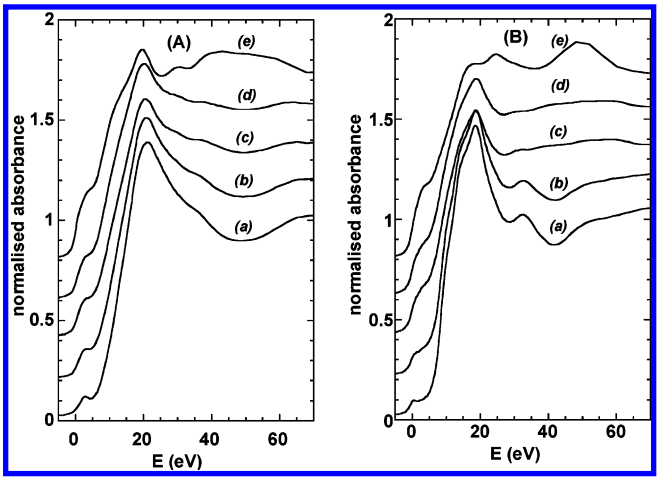

Figure 7. XANES spectra of reduced samples. (A) Fe K-edge of aerogel after reduction at (a) 700 °C for 2 h, (b) 700 °C for 12 h, (c) 800 °C for 12 h, of xerogel after reduction at (d) 800 °C for 2 h, and of (e) bcc Fe. (B) Co K-edge of aerogel after reduction at (a) 700 °C for 2 h, (b) 700 °C for 12 h, (c) 800 °C for 12 h, of xerogel after reduction at (d) 800 °C for 2 h, and of (e) fcc Co.

to the xerogel ones.[19] This difference is probably related to the fact that in the case of FeCo−Al_2O_3 samples both aerogel and xerogel are mesoporous and have similar surface areas,[12,32] whereas in the case of FeCo−SiO_2 samples microporous xerogels and mesoporous aerogels were obtained.[8,9]

In the FTs of the aerogel reduced at 700 °C for 12 h the characteristic features of the bcc phase are still evident at both edges. However, a fraction of the metal is certainly present in the form of oxide phases, as it can be inferred from the shoulder on the left-hand side of the first peak in the FTs. In the aerogel reduced for 2 h at 700 °C a much larger fraction of iron and cobalt is present in some oxide phases. Nevertheless, the presence of a shoulder centered at about 2.5 Å, which is completely absent in the EXAFS FTs of iron and cobalt oxides, indicates that the metal phase is already formed after this treatment, in agreement with XRD.[12]

Figure 7 shows the Fe and Co K-edge XANES of aerogels after reduction at 700 °C for 2 and 12 h and of aerogel and xerogel after reduction at 800 °C for 2 h, and also of bcc Fe and fcc Co foils. After reduction at 700 °C for 2 h the aerogels have Fe and Co K-edge XANES that are similar to those of oxides rather than metals, with clear pre-edge peaks and no inflection points. In fact, the XANES are most similar to those of aerogel after calcination at 450 °C. However, both the Fe and Co K-edge XANES show additional background intensity in the region around the pre-edge peak, and this indicates that some metal is present in addition to oxides. After reduction at 700 °C for 12 h the aerogels still have Fe and Co K-edge XANES that are more similar to those of oxides than metals. However, there is increased background intensity in the region around the pre-edge peak, so the XANES is changing shape toward that of the aerogels reduced at 800 °C for 2 h. This is consistent with the growth of the metal and decline of the oxide phases during reduction at 700 °C for 12 h.

After reduction at 800 °C for 2 h the xerogel and aerogel have similar Co K-edge XANES and also similar Fe K-edge XANES. The Fe and Co K-edge XANES are much more similar to those of metals than oxides, with clear inflection points. The Co K-edge XANES does not have any sign of peaks at 25 and 50 eV, which are obvious for fcc Co, but does have slight rises at 30 and 40 eV, which are apparent for bcc Fe. This indicates the formation of a bcc FeCo alloy. The Fe K-edge XANES has

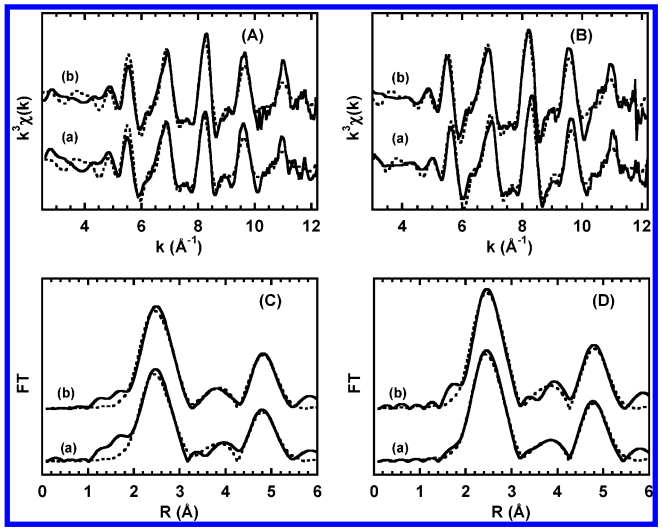

Figure 8. $k^3\chi(k)$ spectra from experiment (—) and fit results (- - -) at the (A) Fe and (B) Co K-edge and corresponding FTs (phase shift corrected) at the (C) Fe and (D) Co K-edge, for the (a) aerogel sample and (b) xerogel sample treated at 800 °C.

a shifted main edge position and an increased intensity in the region of the main edge peak, which indicates the presence of some oxide in addition to metal.

On the basis of the information gathered from the features of the EXAFS and XANES spectra, the fitting of the EXAFS spectra of the aerogel and xerogel samples reduced at 800 °C for 2 h was done using the first five distances of the bcc structure. Calculated phase shift and amplitudes were first checked on the bcc Fe and fcc Co foils.[19] A full multiple scattering calculation was performed since some multiple scattering paths are especially important in the bcc structure, in particular due to the collinear arrangement of the atoms in the first and fifth shell.[26] The fitting was performed using simultaneously the data at the Fe and Co K-edge. Since iron and cobalt have very similar phase shifts and amplitudes, the calculation was simplified by assuming that Fe is surrounded only by Fe and Co is surrounded only by Co. Only R_1, the first Me−Me distance, was fitted, while the distances of the further shells where kept fixed to R_i/R_1 ratios of the bcc structure. All the N_i were kept constant to the typical values of the bcc structure since TEM observations indicated that the average particle size is about 15 nm.[12] Therefore, the reduced amplitude of the EXAFS oscillations of the samples, in comparison with those of bcc Fe foil, was mainly attributed to an increase of the $2\sigma_i^2$. It is well known, in fact, that a significant decrease in coordination numbers is expected only for nanoparticles below 5 nm.[33] To take into account the possibility that some of the Fe atoms are still in oxidized form, as suggested by XANES spectra, the fraction of the central atom in the bcc structure was fitted.

In Figure 8 the results of the fitting at the Fe and Co K-edge are shown for both the aerogel and xerogel samples, and the best fitting parameters are reported in Table 3.

The fitting is good in the actual range of distances used in the fitting, indicating that all the cobalt is reduced, while a fraction of iron, ranging from about 15% for the xerogel to about 19% for the aerogel, is present as an oxide, as a consequence of either an incomplete reduction or a superficial oxidation of the FeCo nanoparticles. The effect of the presence of some oxide is also confirmed by the presence of a shoulder on the left-hand side of the first FT peak at the Fe K-edge, which is slightly more prominent in the aerogel sample, and by the disagreement

TABLE 3: Interatomic Distances (R), Coordination Numbers (N), and Debye−Waller Factors (σ) from Fitting the EXAFS Spectra, Simultaneously at the Fe and Co K-Edge, for the Aerogel and Xerogel Samples Reduced at 800 °C for 2 h

	aerogel		xerogel	
	Fe	Co	Fe	Co
fraction in bcc structure	0.81 (3)	1	0.85 (3)	1

	R (Å)	N	$2\sigma^2$ (Å^2)	R (Å)	N	$2\sigma^2$ (Å^2)
1st shell	2.47 (1)	8	0.018 (6)	2.46 (1)	8	0.018 (6)
2nd shell	2.85	6	0.027 (2)	2.84	6	0.022 (2)
3rd shell	4.03	12	0.027 (3)	4.02	12	0.026 (2)
4th shell	4.73	24	0.030 (3)	4.71	24	0.037 (3)
5th shell	4.94	8	0.030 (3)	4.92	8	0.023 (2)
R-factor		40%			38%	

[a] Errors shown in parentheses for the parameters free to vary during fitting.

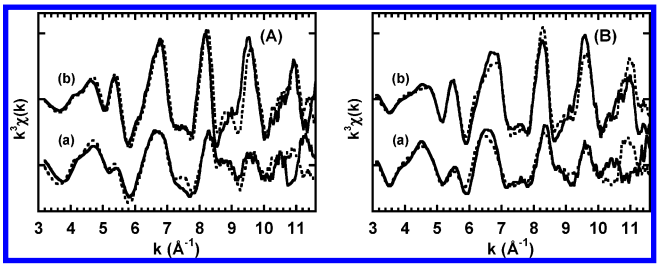

Figure 9. $k^3\chi(k)$ spectra from experiment (—) and linear combination results (- - -) at the (A) Fe and (B) Co K-edge for the aerogel sample treated at 700 °C for (a) 2 h and (b) 12 h.

TABLE 4: Results of the Fitting for the Aerogel Samples Reduced at 700 °C for 2 h and at 700 °C for 12 h Using a Linear Combination of the Spectra of the Aerogel Calcined at 450 °C and Those of the Aerogel Reduced at 800 °C

	700 °C 2 h		700 °C 12 h	
	Fe	Co	Fe	Co
calcined at 450 °C	73%	85%	37%	43%
reduced at 800 °C	27%	15%	63%	57%
R-factor	42%	44%	22%	25%

of the experimental $k^3\chi(k)$ with the fit in the region 2.5−6 Å^{-1} at the Fe K-edge. The Debye−Waller factors of the FeCo alloy nanoparticles are higher than those of the bcc Fe foil,[19] whose typical $2\sigma^2$ range from 0.01 for the first shell up to 0.018 for outer shells, indicating an increase in disorder in the alloy nanocrystals.

The comparison of the data of the aerogels reduced at 700 °C with those of the aerogels calcined at 450 °C and those of the aerogels reduced at 800 °C indicates the presence of a mixture of phases. Since a fitting including both the bcc structure and some oxide phases could include too many free parameters, it seemed sensible to simulate the data of the aerogels reduced at 700 °C with a liner combination of the spectra of the aerogel calcined at 450 °C and those of the samples reduced at 800 °C. To this end, the program LINCOM,[34] which runs a least-squares routine to minimize the difference between one EXAFS spectrum and a combination of up to nine others, was used in the range 2.5−11.5 Å^{-1}. In Figure 9 the results of the linear combination are shown, and in Table 4 the pertinent parameters are reported.

The results of the fitting on the aerogel reduced at 700 °C for 12 h are quite good at both the Fe and Co K-edges, indicating that about 60% of the iron and cobalt are present in the form of

FeCo alloy, while the remaining fraction is still present as oxides. The fitting in the range 2.5−11.5 $Å^{-1}$ is less good for the aerogel reduced at 700 °C for 2 h at both the Fe and Co K-edge, but the *R*-value drops to less than 10% when the upper limit of the fit is lowered to 10 $Å^{-1}$, i.e., excluding the region where the data are noisy and affected by some monochromator glitches. Therefore, these results indicate that about 20% of the iron and cobalt are already present in the form of FeCo alloy nanoparticles, in agreement with XANES observations.

In should be noted that the bcc alloy phase is obtained starting from poorly structured intermediate products that are formed after the calcination treatment at 450 °C. This is quite a different behavior from what was observed in $FeCo-SiO_2$ nanocomposites, where FeCo alloy nanoparticles were obtained via well-discernible phases of iron and cobalt oxide formed as intermediate products.[19]

Conclusion

X-ray absorption spectroscopy was used to separately investigate the iron and cobalt environment in porous sol−gel composites of iron−cobalt−alumina submitted to thermal treatments under oxidizing and reducing conditions. Previous characterization by XRD of the aerogel and xerogel samples calcined at increasing temperature showed only the presence of a single nanocrystalline spinel phase similar to γ-Al_2O_3 and made it therefore difficult to speculate about the structure of the metals in the composite. XANES provides definite indication on the oxidation state of the metals, proving that Co(II) and Fe(III) are present. In agreement, EXAFS data suggest that the iron and cobalt ions are located in tetrahedral sites of a spinel aluminate network. In particular, the iron environment is more disordered, suggesting that Fe(III) ions are spread homogeneously within the matrix. The cobalt environment suggests the presence of more extended $CoAl_2O_4$ domains, which also seem to have a certain degree of inversion. The xerogel sample calcined at 450 °C is definitely more disordered than the aerogel calcined at the same temperature. However, after further calcination at 900 °C, the aerogel and xerogel samples present a very similar structure.

The previous characterization carried out by XRD of the xerogel and aerogel samples treated at high temperature under reducing atmosphere suggested that some metal nanoparticles begin to form in the aerogel after a reduction treatment for 2 h at 700 °C. However, only a weak and broad peak corresponding to the main Bragg reflection of both bcc Fe and fcc Co was detectable, making it quite difficult to understand the real nature of the metal nanoparticles. By taking advantage of the selectivity of the EXAFS technique, a definite confirmation that the bcc FeCo alloy nanoparticles begin to form at 700 °C was obtained. The amount of bcc alloy nanoparticles increases when the reduction at 700 °C is protracted up to 12 h. However, only with a treatment at 800 °C in H_2 flow is the reduction practically complete. No significant difference is observed between the aerogel and the xerogel samples reduced at 800 °C for 2 h.

Acknowledgment. The authors wish to acknowledge the European Community-Access of Research Infrastructure action of the Improving Human Potential Program for accessing the SRS Synchrotron. The Ministero dell'Istruzione, dell'Università e della Ricerca (MIUR-PRIN), and The British-Italian Partnership Programme (British Council-MIUR) are gratefully acknowledged for financial support.

References and Notes

(1) Komarneni, S. *J. Mater. Chem*. **1992**, *2*, 1219.
(2) Fernandez, C. D.; Mattei, G.; Sangregorio, C.; Tagliente, M. A.; Bello, V.; Battaglin, G.; Sada, C.; Tapfer, L.; Gatteschi, D.; Mazzoldi, P. *J. Non-Cryst. Solids* **2004**, *345*−*46*, 681.
(3) Konya, Z.; Vesselenyi, I.; Lazar, K.; Kiss, J.; Kiricsi, I. *Trans. Nanotechnol. IEEE* **2004**, *3*, 73.
(4) Nagaraju, N.; Fonseca, A.; Konya, Z.; Nagy, J. B. *J. Mol. Catal. A: Chem.* **2002**, *181*, 57.
(5) MacLaren, J. M.; Schulthness, T. C.; Butler, B. H.; Sutton, R.; McHenry, M. *J. Appl. Phys.* **1999**, *85*, 4833.
(6) Saad, A. M.; Mazanik, A. V.; Kalinin, Yu. E.; Fedotova, J. A.; Fedotov, A. K.; Wrotek, S.; Sitnikov, A. V.; Svito, I. A. *Rev. Adv. Mater. Sci.* **2004**, *8*, 152.
(7) Brinker, C. J.; Scherer, G. W. *Sol-gel Science*; Academic Press: San Diego, 1990.
(8) Ennas, G.; Casula, M. F.; Falqui, A.; Gatteschi, D.; Marongiu, G.; Piccaluga, G.; Sangregorio, C.; Pinna, G. *J. Non-Cryst. Solids* **2001**, *293*−*295*, 1.
(9) Casula, M. F.; Corrias, A.; Paschina, G. *J. Mater. Chem.* **2002**, *12*, 1505.
(10) Casula, M. F.; Corrias, A.; Falqui, A.; Serin, V.; Gatteschi, D.; Sangregorio, C.; de Julián Fernández, C.; Battaglin, G. *Chem. Mater.* **2003**, *15*, 2201.
(11) Ennas, G.; Falqui, A.; Marras, S.; Sangregorio, C.; Marongiu, G. *Chem. Mater.* **2004**, *16*, 5659.
(12) Corrias, A.; Casula, M. F.; Falqui, A.; Paschina, G. *Chem. Mater.* **2004**, *16*, 3130.
(13) Koningsberger, D. C.; Prins, R. *X-ray Absorption. Principles, Applications, Techniques of EXAFS, SEXAFS and XANES*; Wiley: New York, 1988.
(14) Moscovici, J.; Michalowicz, A.; Decker, S.; Lagadic, I.; Latreche, K.; Klabunde, K. *J. Synchrotron Rad.* **1999**, *6*, 604.
(15) Moscovici, J.; Benzakour, M.; Decker, S.; Carnes, C.; Klabunde, K.; Michalowicz, A. *J. Synchrotron Radiat.* **2001**, *8*, 925.
(16) Chadwick, A. V.; Mountjoy, G.; Nield, V. M.; Poplett, I. J. F.; Smith, M. E.; Strange, J, H.; Tucker, M. G. *Chem. Mater.* **2001**, *13*, 1219.
(17) Corrias, A.; Mountjoy, G.; Piccaluga, G.; Solinas, S. *J. Phys. Chem. B* **1999**, *103*, 10081.
(18) Corrias, A.; Ennas, G.; Mountjoy, G.; Paschina, G. *Phys. Chem. Chem. Phys.* **2000**, *2*, 1045.
(19) Corrias, A.; Casula, M. F.; Ennas, G.; Marras, S.; Navarra, G.; Mountjoy, G. *J. Phys. Chem. B* **2003**, *107*, 3030.
(20) Grunes, L. A. *Phys. Rev. B* **1983**, *27*, 2111
(21) Klementiev, K. V. *Appl. Phys.* **2001**, *34*, 209.
(22) Binsted, N. *EXCURV98: CCLRC Daresbury Laboratory computer program*; 1998.
(23) von Barth, U.; Hedin, L. *J. Phys. C* **1972**, *5*, 1629.
(24) Crozier, E. D. *Nucl. Instrum. Method Phys. Res. B* **1997**, *133*, 134.
(25) Gurman, S. J.; Binsted, N.; Ross I. *J. Phys. C* **1984**, *17*, 143.
(26) Teo, B. K. *J. Am. Chem. Soc.* **1981**, *103*, 3990.
(27) Rehr, J. J.; Albers, R. C. *Phys. Rev. B* **1990**, *41*, 8139.
(28) Rehr, J. J.; Albers, R.C.; Zabinsky, S. I. *Phys. Rev. Lett.* **1992**, *69*, 3397.
(29) Error Report of the International XAFS Society Standards and Criteria Committee, 2000 (*http://ixs.iit.edu/subcommittee_reports/sc/*).
(30) Bianconi, A. In *X-ray absorption: principles, applications, techniques of EXAFS, SEXAFS and XANES*; Koninbsberger, D. C., Prins, R., Eds.; Wiley: New York, 1987; Chapter 11.
(31) Christensen, A. N.; Norby, P.; Hanson, J. C. *Powder Diffr.* **1995**, *10*, 185.
(32) Ennas, G.; Marras, S. Private communication.
(33) Greegor, R. B.; Lytle, F. W. *J. Catal.* **1980**, *63*, 476.
(34) *LINCOM*, Linear combination program from CCP3, Collaborative Computational Project 3; Daresbury Laboratory: U.K.